

ANISOTROPY IN TENSILE PROPERTIES OF ADVANCED SILICON CARBIDE COMPOSITES—T. Nozawa, Y. Katoh (Oak Ridge National Laboratory), and R. J. Shinavski (Hyper-Therm High-Temperature Composites, Inc.)

OBJECTIVE

The objective of this study is to evaluate the anisotropy in tensile properties of nuclear-grade SiC/SiC composites to provide a basis for the practical component design.

SUMMARY

This study evaluates the anisotropy in tensile properties of satin-woven (S/W) or biaxially braided Hi-Nicalon™ Type-S fiber reinforced chemical-vapor-infiltrated (CVI) SiC matrix composites with multilayered interphase. Results indicate excellent axial and off-axis tensile fracture behaviors for the S/W composites. In contrast, the braided composites failed at unexpectedly lower stresses. The primary cause for this difference was the varied in-plane shear properties, on which off-axis tensile properties significantly depend. Superior in-plane shear properties for the S/W composites were achieved by increasing the volume fraction of transverse fibers normal to the fracture plane. Considering the failure modes depend on the off-axis angle, the anisotropy in proportional limit tensile stress and fracture strength were satisfactorily predicted by a simple stress criterion model. The anisotropy in Young's modulus was well-described by a conventional rule of mixtures for laminates. It is worth noting that specimen size effect on axial and off-axis tensile properties seems very minor for nuclear-grade SiC/SiC composites with rigid CVI-SiC matrix.

PROGRESS AND STATUS

Introduction

Silicon carbide (SiC) ceramics and composites are candidate materials for advanced fission and nuclear fusion applications due to several characteristics such as excellent stability of strength and thermal properties at elevated temperatures, chemical inertness, low radiation-induced activation and low after-heat. Additionally, a crystalline, high-purity, and stoichiometric SiC form such as chemically-vapor-deposited (CVD) SiC provides superior irradiation resistance, e.g., good strength retention [1], improved fracture toughness [2, 3], and moderate thermal transport properties under irradiation [4]. It is now recognized that nuclear-grade SiC/SiC composites reinforced by highly-crystalline and near-stoichiometric "Generation III" SiC fibers, i.e., Hi-Nicalon™ Type-S or Tyranno™-SA, with the high-quality SiC matrix, are similarly radiation-damage resistant [5–7]. Due to the recent advances of composite fabrication techniques and optimization of the fiber/matrix interface, remarkable improvement of the composite performance and reliability under neutron irradiation has been achieved [8].

One of the important design aspects for the use of composites is fiber architecture to ensure the best optimized margins against stresses generated by mechanical loading or thermal expansion in the axial and hoop directions, i.e., anisotropy. Multi-axial fiber reinforcement is often applied to mitigate the issue of anisotropic properties. Historically, studies on anisotropic tensile fracture behaviors of conventional SiC/SiC composites have been conducted [9, 10]. For advanced SiC/SiC composites with rigid matrix such as CVI-SiC, understanding the mechanical contribution from the matrix as well as the fiber should be essential since the rigid SiC matrix enables to transfer load as large as the reinforcing fiber can. Also, the role of the fiber/matrix interface should be emphasized.

Experimental Procedure

Nuclear-grade SiC/SiC composites with different fiber architectures were fabricated by Hyper-Therm High-Temperature Composites, Inc. (Huntington Beach, CA) and their key characteristics are summarized in Table 1. The reinforcement fiber was Hi-Nicalon™ Type-S and the matrix was CVI-SiC. The fiber bundles were biaxially braided for NG1 and NG2, or satin-woven for NG3. The off-axis angle was $\pm 55^\circ$ for NG1 and

$\pm 53^\circ$ for NG2. A multilayered interface composed of a sequence of pyrolytic carbon (PyC) and CVI-SiC was formed on the fiber. The carbon adjacent to the fiber has a thickness of ~ 150 nm, while the other 4 surrounding layers have a thickness of ~ 20 nm. The thickness of the SiC inserts between carbon interlayers was ~ 100 nm. The density of NG1 braid composites was ~ 2.9 g/cm³, while the density of NG2 braid was ~ 2.7 g/cm³. Due to the high density of the NG1 braid, the porosity, V_p , of the NG1 braid was quite low, $\sim 9\%$, although the NG2 composites possess the porosity of $\sim 16\%$. The density and porosity of the NG3 S/W composites were ~ 2.7 g/cm³ and $\sim 16\%$, respectively. The total fiber volume fraction of 30~40% was designed for each material.

Table 1. Material properties of SiC/SiC composites tested

Material	ID	Loading axis	Density [g/cm ³]	Fiber Volume Fraction	Porosity
NG1 Biaxial braid [$\pm 55^\circ$]	Braid-35	Transverse	2.87	~ 0.3	0.09
	Braid-55	Axial	2.83	~ 0.3	0.08
NG2 Biaxial braid [$\pm 53^\circ$]	Braid-53	Axial	2.62	~ 0.3	0.16
NG3 Satin-weave [$0^\circ/90^\circ$]	S/W-0/90	Axial	2.69	~ 0.4	0.14
	S/W-45	45° off-axis	2.61	~ 0.4	0.16

Room-temperature tensile tests were performed following general guidelines of ASTM C1275-00. Two types of tensile specimens: a face-loaded straight bar specimen and an edge-loaded contoured specimen were used (Fig. 1). To investigate the effect of specimen size on tensile properties, the gauge width was varied from 4.0 to 15.0 mm. Sub-sets of tensile tests were conducted accompanied with unloading/reloading cycles to evaluate the hysteresis response. Tensile strain was measured using a pair of strain gauges bonded in the middle gauge section of the specimen. The length of the strain gauges was 5.0 mm. For off-axis tensile tests, 90° -axis (transverse) and 45° -axis strains as well as 0° -axis (axial) strain were measured to determine the in-plane shear strain. A constant crosshead displacement rate of 0.5 mm/min was applied. Fracture surfaces were observed by the scanning electron microscopy.

In advance of tensile tests, dynamic Young's modulus was measured by the sonic resonance method according to ASTM C1259-01 only for straight bar specimens.

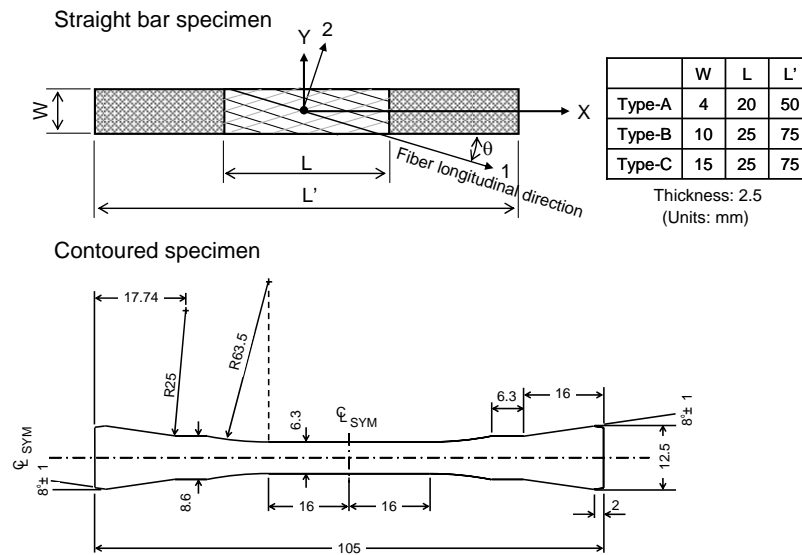


Fig. 1. Schematic illustrations of tensile specimens.

Results and Discussion

Tensile fracture behavior

Figure 2 exhibits typical tensile stress-strain curves of the SiC/SiC composites tested. The tensile Young's modulus of the composites was defined as a tangential modulus from the initial linearity. The proportional limit tensile stress (PLS) was defined by the 5% deviation from linearity method. The tensile strength was defined as a failure load divided by the original gauge cross-section. Experimental errors indicated were deviation from the maximum or the minimum due to the scarce of valid tests, while scatter of dynamic Young's modulus means \pm one standard deviation. The reduced data were summarized in Table 2.

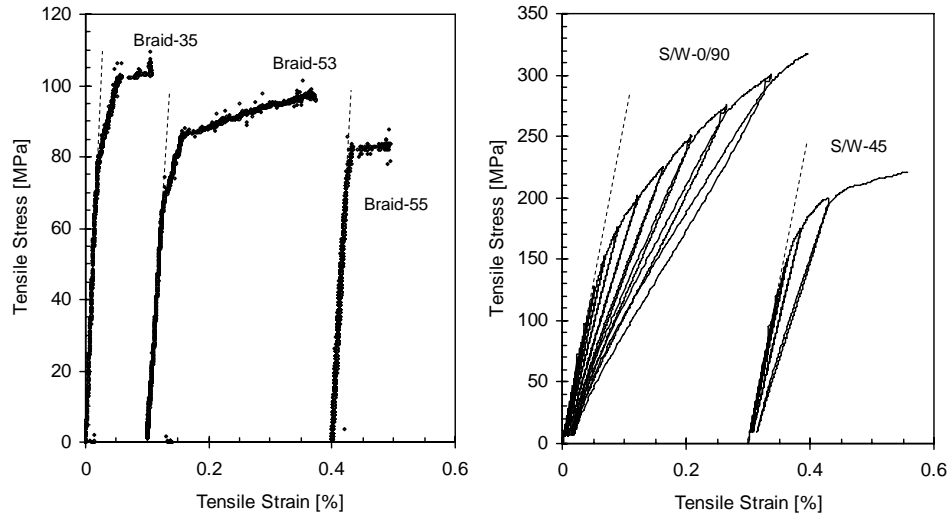


Fig. 2. Typical tensile stress-strain curves of advanced SiC/SiC composites.

Table 2. Tensile properties of advanced SiC/SiC composites

ID	Spec. type (Gauge width)	# of valid tests	Dynamic Young's modulus [GPa]	Tensile Young's modulus [GPa]	PLS [MPa]	Tensile strength [MPa]	Fracture strain [%]
Braid-35	Straight bar (10.0 mm)	3	314 \pm 1	369 +49/-66	68 +12/-6	105 +2/-1	0.16 +0.09/-0.05
Braid-55	Straight bar (4.0 mm)	3	338 \pm 6	302 +101/-73	86 +16/-18	87 +15/-19	0.03 +0.02/-0.01
	Contoured (6.3 mm)	4	-	237 +16/-13	79 +8/-8	82 +8/-9	0.04 +0.01/-0.01
	Straight bar (10.0 mm)	4	290 \pm 19	315 +62/-49	75 +3/-9	78 +6/-7	0.10 +0.15/-0.07
	Straight bar (15.0 mm)	2	282 \pm 0	395 +9/-9	82 +4/-4	91 +1/-1	0.04 +0.01/-0.01
Braid-53	Straight bar (10.0 mm)	5	218 \pm 12	174 +88/-55	62 +8/-7	108 +11/-11	0.51 +0.10/-0.24
S/W-0/90	Straight bar (4.0 mm)	9	276 \pm 9	277 +7/-11	111 +21/-19	346 +67/-50	0.34 +0.05/-0.05
	Contoured (6.3 mm)	4	-	256 +38/-26	114 +7/-10	348 +29/-43	0.62 +0.07/-0.12
S/W-45	Straight bar (4.0 mm)	5	232 \pm 11	248 +12/-32	136 +10/-9	206 +15/-32	0.33 +0.23/-0.24
	Contoured (6.3 mm)	4	-	232 +18/-32	102 +12/-14	206 +7/-4	0.44 +0.06/-0.07

Satin-woven composites (NG3) show superior tensile fracture behaviors coupled with graceful unloading/reloading hysteresis curves. The tensile strength of S/W-0/90 was quite high over 300 MPa. Due primary to the anisotropy issue, the S/W-45 failed at a lower fracture stress (~210 MPa) than obtained in the axial tests. For both S/W-0/90 and S/W-45, the considerably high PLS (~130 MPa) was obtained. Meanwhile, NG1 and NG2 braid composites show comparably low tensile strength (~110 MPa) and PLS (~80 MPa). The major difference between NG1 and NG2 composites is the magnitude of failure strain. The failure strain for NG2 was significant (~0.51%), while most of NG1 failed by first matrix cracking at the proportional limit (0.03~0.16%). Although the NG1 braid composites with the dense matrix recorded the highest Young's modulus (~310 GPa), they were within the same magnitude.

It is worth noting that no major size effect seems anticipated in the specimen size range of this study. The effect of specimen size and geometry on axial and off-axis tensile properties for PIP SiC/SiC composites was reported by the authors [11]. The key conclusions of this study are 1) no systematic length, width and thickness effects on axial tensile properties if the fiber volume fraction in the loading direction in a unit structure is unchanged by specimen size, 2) the size dependency of off-axis tensile properties due to the size-relevant change of fracture modes, and 3) very minor effect of specimen geometry. The in-plane shear strength and detachment strength of the low-stiffness PIP-SiC matrix composites are inherently low. Additionally, very narrow specimens show much lower in-plane shear properties due to the size effect. A probable explanation for no major systematic size effect observed for advanced SiC/SiC composites is improved in-plane shear properties of the Generation III dense and rigid matrix composites as discussed later. It is speculated that high load transferability at the fiber/matrix interface can achieve superior in-plane shear properties for any size of specimens.

Figure 3 shows typical tensile fracture surfaces. The figure does not list fracture surfaces of Braid-35 due to the similarity with those of Braid-55. Generally, the fracture plane of the off-axis tensile specimens except for some of the Braid-35 and Braid-55 composites was parallel to the longitudinal fiber direction, although this does not conclude brittle fracture. It is obvious that there exist fiber pullouts on the fracture surface. Specifically bluish-like fibers for S/W-45 indicate progressive debonding of transverse fibers normal to the fracture plane. Besides, major cracks propagated within the fiber bundles for Braid-53. These facts promise the in-plane shear as a primary fracture mode in off-axis tension. In contrast, the first matrix cracking behavior seems dominate a failure of NG1 braid composites, the fracture surface of which shows small amounts of very short fiber pullouts embedded in rich SiC matrix, causing a brittle-like fracture. The fracture surface of S/W-0/90 was very fibrous coupled with significant transverse cracks in

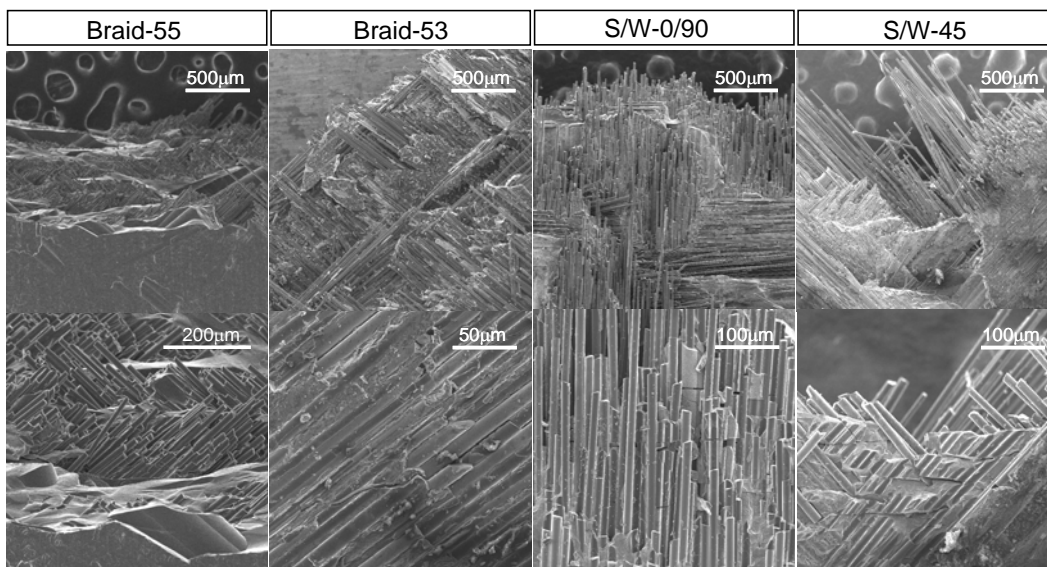


Fig. 3. Typical fracture surface images of SiC/SiC composites.

the 0°- bundles with an average crack spacing of ~25 μm . Similarly, very limited amounts of transverse cracks were observed for S/W-45. However, they were very minor and most of them were localized near the cross sections of the 45°-bundles.

Damage accumulation process

The damage parameter defined in Ref. 12, which is proportional to crack density, was first induced beyond the proportional limit (110~140 MPa) and rapidly increased when the applied stress exceeded ~165 MPa for both S/W-0/90 and S/W-45 (Fig. 4). In contrast, both loop width and inelastic strain index (L) were initiated at the stress of ~165 MPa and they increased monotonically with increasing applied stress. For a [0°/90°] fiber configuration, it is well-known that the damage accumulation first occurs by cracking in the 90°-bundles and then the 90°-bundle cracks extend to form transverse cracks, i.e., matrix cracking (in some paper this is referred to as tunnel cracking), in the 0°-bundles [13,14]. Accordingly, the stress to initiate matrix cracking, σ_{mc} , can be estimated as a stress at $L = 0$, i.e., $\sigma_{mc} = 165$ MPa. Since damages in composites rapidly increase beyond the materials proportional limit, the transverse cracking for S/W-0/90 generally occurred at lower stress than that of undamaged unidirectional (UD) composites (~230 MPa). In contrast, it is speculated that the secondary damage for S/W-45 was caused by the combined effect of in-plane shear and fiber detachments coupled with fiber sliding at the debonded fiber/matrix interface. Therefore, the similar analysis is not presently guaranteed for the off-axis tensile data.

Applying a mean matrix crack spacing of ~25 μm yields an estimated interfacial friction stress of ~100 MPa for S/W-0/90. This is within the same range obtained by the single fiber push-out test for UD Hi-Nicalon™ Type-S/CVI-SiC composites [15]. The high interfacial friction stress may contribute significantly to stress transferring at the interface during fiber pullout process.

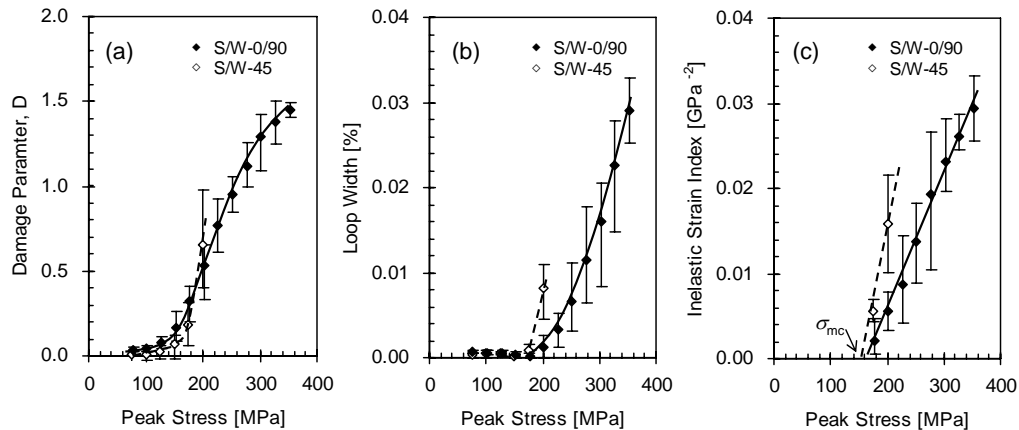


Fig. 4. (a) damage parameter, (b) loop width, and (c) inelastic strain index.

In-plane shear properties

Off-axis tensile tests provide in-plane shear fracture behavior by simple stress conversion [16]. Figure 5 shows in-plane shear stress vs. shear strain curves for S/W-45 and Braid-53. The non-linear segment followed by the initial linearity indicates failure with mixed fracture modes: in-plane shear and fiber detachment coupled with fiber pullouts of transverse fibers. In Fig. 5, the lower proportional limit shear stress (~30 MPa) and shear failure stress (~55 MPa) for Braid-53 were obvious, while the proportional limit shear stress and the shear strength for S/W-45 were ~50 MPa and ~100 MPa, respectively. The in-plane shear properties were slightly improved for braid composites and considerably improved for S/W composites, compared with a proportional limit shear stress of ~15 MPa and a shear failure strength of ~50

MPa for early generation SiC/SiC composites reinforced by Tyranno™-LoxM Si-Ti-C-O fibers with the poor stiffness SiC matrix fabricated by the polymer impregnation and pyrolysis (PIP) process [11].

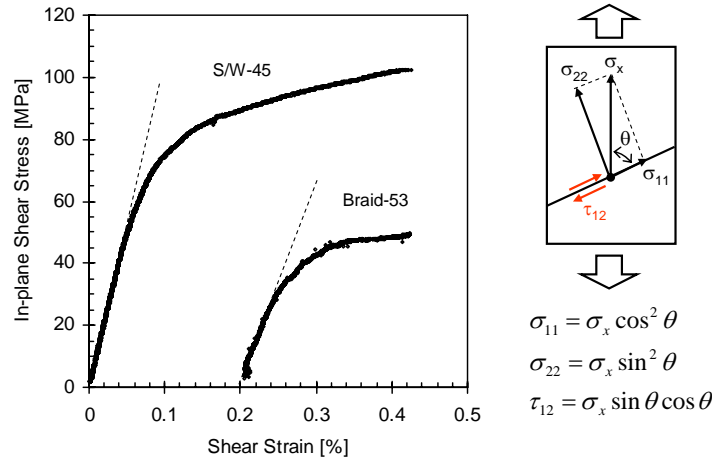


Fig. 5. In-plane shear stress vs. shear strain.

The higher proportional limit shear stress (~55 MPa) and in-plane shear fracture strength (~100 MPa) for S/W-45 resulted in the superior off-axis tensile properties. It is obvious that the contribution from continuous fibers aligned perpendicular to the shear fracture plane is extraordinary for biaxial (including satin-woven) composites. Specifically, the high interfacial friction (~100 MPa) for nuclear-grade SiC/SiC composites can allow significant load transfer via the fiber/matrix interface beyond first in-plane shear cracking. Denk et al. [17] specified the effect of the volume fraction of transverse fibers on in-plane shear strength by Iosipescu shear testing of carbon/carbon composites. A high fiber volume fraction in a unit structure was achieved due probably to the tightly-woven architecture for S/W-45. Therefore, it is reasonable to conclude that S/W-45 with a slightly higher fiber volume fraction of ~40% exhibits the higher in-plane shear properties. Additionally, the pore distribution would affect the in-plane shear data. The braid composites preferably possess pocket pores between fiber bundles however the effect of pocket pores might be minor for the dense NG1 braid composites.

Anisotropy of tensile properties

Continuous fiber reinforcement of the composites provides higher reliability in fracture behaviors as compared with those of brittle ceramics, however, simultaneously imposes anisotropy on material properties. In Figs. 6 and 7, the anisotropy of tensile properties was summarized. For comparison, tensile data of the Generation III SiC/SiC composites in literature were also included.

Figure 6 shows the tensile Young's modulus with respect to the off-axis angle, θ . The Young's modulus of the composites exhibits the maximum at $\theta = 0$ and it tends to decrease with increasing off-axis angle. The anisotropy of the Young's modulus has long been discussed and the composite modulus can be well-described by a rule of mixtures for laminates [20]. Assuming a UD fiber configuration with a fiber volume fraction of 0.3 and varied porosity ranged from 5–20%, an anisotropic change of the Young's modulus can be predicted as shown in Fig. 6. Note that the model assumes columnar pores distributed along the fiber bundles. Analytical results clearly indicate that the Young's modulus decreases with increasing porosity. The data of dense NG1 braid composites agreed with the analytical trend very well, although the moduli for the other composites with a porosity of ~16% did not. Underestimating the porosity effect may result in the lower Young's moduli for the porous composites. Besides columnar pores, there exist pores distributed in pockets at the cross-points of fiber bundles for braid and woven composites.

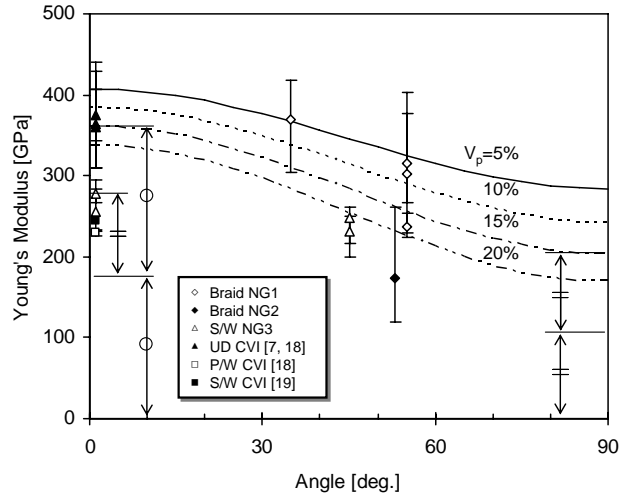


Fig. 6. Anisotropy of Young's modulus. Young's moduli for unidirectional composites with a fiber volume fraction of 30% and varied porosity ($V_p = 5\text{--}20\%$) are predicted by a conventional rule of mixtures (solid and broken lines).

Figure 7(a) shows PLS with respect to the off-axis angle. Key crack initiation mechanisms are supposed to be 1) transverse cracking perpendicular to the fiber longitudinal direction, i.e., matrix cracking, 2) in-plane shear cracking within the fiber bundles along the longitudinal fibers, and 3) interlaminar shear cracking along the longitudinal fibers by fiber detachment. For off-axis tension, the applied stress can be separated into three stress elements: tensile stresses in the longitudinal fiber direction, $\sigma_{11} (= \sigma_x \cos^2(\theta))$, and in the transverse fiber direction, $\sigma_{22} (= \sigma_x \sin^2(\theta))$, and in-plane shear stress on the plane parallel to the longitudinal fiber direction, $\tau_{12} (= \sigma_x \sin(\theta) \cos(\theta))$. For simplicity, we assume a critical stress to initiate matrix cracking, i.e., transverse cracking in 0° -bundles, as $\sigma_{11} = 230$ MPa from the result of UD composites

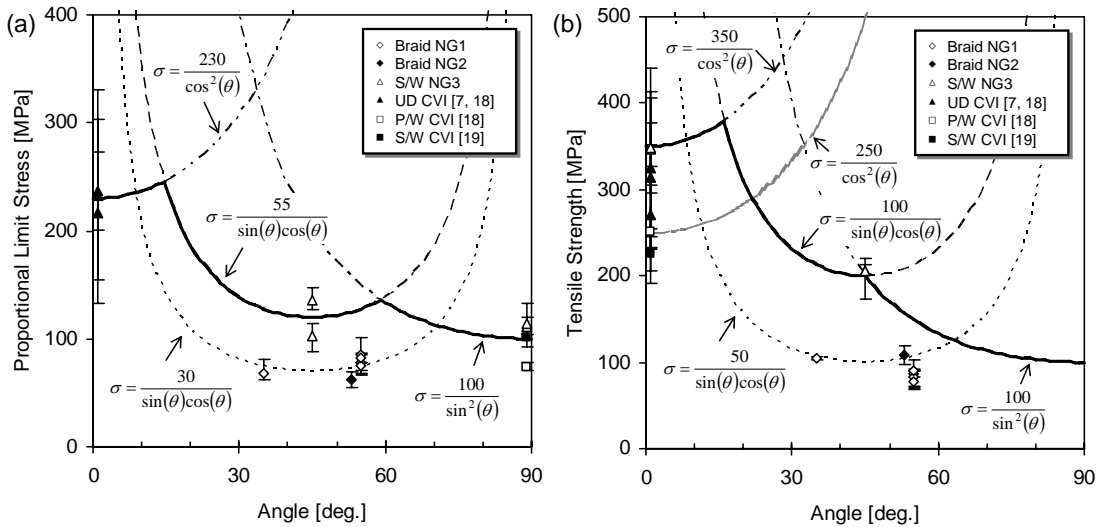


Fig. 7. Anisotropy of (a) PLS and (b) tensile strength. Estimates of PLS and tensile strength are also plotted. The stress criterion for NG3 S/W composites was, for instance, shown as a solid line in the figures.

and a critical detachment stress as $\sigma_{22} = 100$ MPa taking a PLS of $[0^\circ/90^\circ]$ composites. A critical in-plane shear stress to induce first cracking is equivalent to a proportional limit shear stress obtained from Fig. 5 ($\tau_{12} = 30$ MPa for NG1 and NG2 vs. $\tau_{12} = 55$ MPa for NG3). Assuming a unique fracture mode operated, stress criterion to determine PLS is therefore drawn as shown in Fig. 7(a). The high PLS for NG3 S/W composites was due to the high proportional limit shear stress to initiate a parallel crack in the fiber bundles. Large scatter of PLS data at $\theta = 0$ seems as a consequence of scattered fiber volume fraction.

Similar to the PLS case, a fracture mechanism anisotropy map for tensile strength can be defined in Fig. 7(b). The critical in-plane shear fracture strengths of 50 MPa for both braid composites, and 100 MPa for NG3, were derived in Fig. 5. The detachment failure strength is assumed to be identical with a detachment initiation stress of ~ 100 MPa. This is a reasonable assumption since the trans-thickness tensile specimen generally fails without a non-linear damage accumulation stage [21]. Large scatter of tensile strength for UD composites ($\theta = 0$) was due to scatter of the axial fiber volume fraction in the cross-section. It is well-known that the composite fracture strength depends significantly on the axial fiber volume fraction [22]. As infer from Fig. 7(b), there exists the co-operation of multiple failure modes for S/W-45. In contrast, the failure mode of braided composites appears only in-plane shear, although the failure behavior beyond the proportional limit was quite different in each braid composite as discussed.

Acknowledgement

This work was sponsored by the Office of Fusion Energy Sciences, U.S. Department of Energy, under contract DE-AC05-00OR22725 and by the Office of Nuclear Energy Science and Technology, U.S. Department of Energy, under contract DE-AC05-00OR22725 with UT-Battelle, LLC.

References

- [1] Y. Katoh and L. L. Snead, J. ASTM Int. 2 (2005) JAI12377.
- [2] S. Nogami, A. Hasegawa, and L. L. Snead, J. Nucl. Mater. 307–311 (2002) 1163.
- [3] Y. Katoh, private communication.
- [4] L. L. Snead, J. Nucl. Mater. 329–333 (2004) 524.
- [5] L. L. Snead, Y. Katoh, A. Kohyama, J. L. Bailey, N. L. Vaughn, and R. A. Lowden, J. Nucl. Mater. 283–287 (2000) 551.
- [6] J. B. J. Hegeman, J. G. van der Laan, M. van Kranenburg, M. Jong, D. d'hulst, and P. ten Pierick, Fusion Eng. Des. 75–79 (2005) 789.
- [7] Y. Katoh, T. Nozawa, L. L. Snead, and T. Hinoki, 12th International Conference on Fusion Reactor Materials, 2005, Santa Barbara, Calif., USA, Journal of Nuclear Materials (accepted).
- [8] Y. Katoh, L. L. Snead, C. H. Henager, Jr., A. Hasegawa, A. Kohyama, B. Riccardi, and H. Hegeman, 12th International Conference on Fusion Reactor Materials, 2005, Santa Barbara, Calif., USA, Journal of Nuclear Materials (accepted).
- [9] C. Cady, F. E. Heredia, and A. G. Evans, J. Am. Ceram. Soc. 78 (1995) 2065.
- [10] T. Nozawa, Y. Katoh, A. Kohyama, and E. Lara-Curzio, 25th Annual International Conference on Advanced Ceramics & Composites, 2001, Cocoa Beach, Fla., USA.
- [11] T. Nozawa, Y. Katoh, and A. Kohyama, Mater. Trans. 46 (2005) 543.
- [12] E. Vagaggini, J.-M. Domergue, and A. G. Evans, J. Am. Ceram. Soc. 78 (1995) 2709.
- [13] Z. C. Xia, R. R. Carr, and J. W. Hutchinson, Acta Metal. Mater. 41 (1993) 2365.
- [14] Z. C. Xia and J. W. Hutchinson, Acta Metal. Mater. 42 (1994) 1933.
- [15] T. Nozawa, Y. Katoh, and L. L. Snead, 12th International Conference on Fusion Reactor Materials, 2005, Santa Barbara, Calif., USA, Journal of Nuclear Materials (accepted).
- [16] W. R. Broughton, Shear, Mechanical Testing of Advanced Fibre Composites, J. M. Hodgkinson (ed.), Woodhead Publishing Limited, Cambridge, England, 2000, 1001–1023.
- [17] L. Denk, H. Hatta, A. Misawa, and S. Somiya, Carbon 39 (2001) 1505.
- [18] T. Nozawa, unpublished work.
- [19] T. Nozawa, Y. Katoh, L. L. Snead, T. Hinoki, and A. Kohyama, 29th International Conference of Advanced Ceramics and Composites, 2005, Cocoa Beach, Fla., USA.

- [20] T. Ishikawa, K. Bansaku, N. Watanabe, Y. Nomura, M. Shibuya, and T. Hirokawa, *Compos. Sci. Technol.* 58 (1998) 51.
- [21] Y. Maki, T. Hinoki, and A. Kohyama, 29th International Conference of Advanced Ceramics and Composites, 2005, Cocoa Beach, Fla., USA.
- [22] W. A. Curtin, *J. Am. Ceram. Soc.* 74 (1991) 2837.